Ionizing radiation predisposes non-malignant human mammary epithelial cells to undergo TGFβ- induced epithelial to mesenchymal transition

Kumari L Andarawewa, Anna C Erickson, William S Chou, Sylvain V Costes, Philippe Gascard, Joni D Mott, Mina J Bissell and Mary Helen Barcellos-Hoff

Life Sciences Division, Lawrence Berkeley National Laboratory, Berkeley, CA 94720

*Corresponding Author: M.H. Barcellos-Hoff

Life Sciences Division
Bldg. 977-225A
1 Cyclotron Rd.
Berkeley, CA 94720
510-486-6371 PHONE
510-486-5586 FAX
MHBarcellos-Hoff@lbl.gov

Financial Support: Support was provided by National Aeronautics and Space Administration Specialized Center for Research in Radiation Health Effects; the Low Dose Radiation Program of the DOE Office of Biological Effects Research; DOD DAMD17-00-1-0224 to ACE; and the Office of Health and Environmental Research, Health Effects Division, United States Department of Energy (contract no.03-76SF00098).

Running Title: Radiation-induced EMT

Total Word Count: 7661

Abstract: 241

Text: 4585

Figures: 6

Key Words: TGFβ, ionizing radiation, mammary epithelial cell, EMT

Abbreviations:

Transforming growth factor β1, TGFβ; ionizing radiation, IR; human mammary epithelial cells, HMEC; epidermal growth factor, EGF; epithelial to mesenchymal transition, EMT; conditioned medium, CM.

Abstract

Transforming growth factor β1 (TGFβ) is a tumor suppressor during the initial stage of tumorigenesis, but it can switch to a tumor promoter during neoplastic progression. Ionizing radiation (IR), both a carcinogen and a therapeutic agent, induces TGFβ activation *in vivo*. We now show that IR sensitizes human mammary epithelial cells (HMEC) to undergo TGFβ-mediated epithelial to mesenchymal transition (EMT). Non-malignant HMEC (MCF10A, HMT3522 S1 and 184v) were irradiated with 2 Gy shortly after attachment in monolayer culture, or treated with a low concentration of TGFβ (0.4 ng/ml), or double-treated. All double-treated (IR+TGFβ) HMEC underwent a morphological shift from cuboidal to spindle-shaped. This phenotype was accompanied by decreased expression of epithelial markers E-cadherin, β-catenin and ZO-1, remodeling of the actin cytoskeleton, and increased expression of mesenchymal markers N-cadherin, fibronectin and vimentin. Furthermore, double-treatment increased cell motility, promoted invasion and disrupted acinar morphogenesis of cells subsequently plated in Matrigel™. Neither radiation nor TGFβ alone elicited EMT, even though IR increased chronic TGFβ signaling and activity. Gene expression profiling revealed that double treated cells exhibit a specific 10-gene signature associated with Erk/MAPK signaling. We hypothesized that IR-induced MAPK activation primes non-malignant HMEC to undergo TGFβ-mediated EMT. Consistent with this, Erk phosphorylation were transiently induced by irradiation, persisted in irradiated cells treated with TGFβ, and treatment with U0126, a Mek inhibitor, blocked the EMT phenotype. Together, these data demonstrate that the interactions between radiation-induced signaling pathways elicit heritable phenotypes that could contribute to neoplastic progression.

Introduction

An emerging concept in cancer biology is that carcinogens can compromise tissue integrity by eliciting altered phenotypes and tissue composition (reviewed in (1)). Intercellular and extracellular signals are critical to the suppression of neoplastic growth while disruption of cell–cell and cell-matrix interactions is implicated, if not required, for neoplastic progression. Indeed, reversion of the malignant phenotype by modulating extracellular signals suggests that cancer cells are susceptible to signals from the microenvironment (2).

We have postulated that ionizing radiation (IR) alters cell phenotypes, that in turn contribute, directly or indirectly, to carcinogenesis (3). IR activates multiple signaling pathways depending on the cell type, radiation dose and cell status (reviewed in (4)). IR also affects the activity or abundance of proteases, growth factors, cytokines, and adhesion proteins that are involved in tissue remodeling (reviewed in (5)). We have shown that transforming growth factor β1 (TGFβ) is activated following IR, and that it in turn mediates cellular and tissue radiation responses (6, 7). Although TGFβ is considered to be a potent tumor suppressor during the initial stage of tumorigenesis, principally through its ability to cause growth arrest and apoptosis, numerous reports show that TGFβ can switch to tumor promoter during neoplastic progression (reviewed in (8)). We have shown that the progeny of irradiated non-malignant human mammary epithelial cells (HMEC) cultured with TGFβ exhibit compromised morphogenesis, polarity and growth control when cultured in reconstituted basement membrane (9).

Some epithelial tumors, particularly those that overexpress TGFβ (10), exhibit mesenchymal characteristics and are more aggressive. Several lines of evidence have led researchers to link this morphological shift during carcinogenesis to the physiological process of epithelial to mesenchymal transition (EMT). EMT is characterized by loss of epithelial cell polarity, loss of cell-cell contacts, acquisition of mesenchymal markers and phenotypic traits that include increased cell motility (reviewed in (11)). Although the clinical relevance of EMT in late-stage tumor progression is controversial, it is generally agreed that EMT can occur during cancer progression (11). Approximately 18% of breast cancers exhibit evidence of EMT (12). EMT has recently been reported during tumor recurrence after therapy (13). TGFβ has been particularly targeted as a mediator of EMT during neoplastic progression, but analysis of normal epithelial and cancer cell lines showed that TGFβ alone rarely induces EMT by (14).

In the present studies, we found that a single exposure to IR sensitizes HMEC to undergo TGFβ-mediated EMT and exhibit all the classic hallmarks of EMT. Neither irradiation nor TGFβ alone was sufficient to elicit EMT even though TGFβ activity is elevated in irradiated cells. Gene expression profiling revealed a specific signature in double-treated cells associated with MAPK signaling. As previously reported, IR induces transient activation of the MAPK pathway, but exposure to low concentrations of TGFβ maintains this pathway activity, which is required for maintenance of EMT. We postulate that the pathway signaling interactions between radiation-induced MAPK and TGFβ elicit the heritable EMT phenotype.

Materials and Methods

Cell culture: HMEC were cultured in serum free medium as previously described for HMT-3522 S1 (S1; passages 55-60) (15), MCF10A (ATCC, Manassas,VA), 184 HMEC (184v; passage 7-10) (16) and HMT-3522-S2 (S2) (17). Recombinant human TGFβ 1 (0.4 ng/ml) was added at the time of plating or of irradiation. HMEC were irradiated 4-5h (S1, MCF10A and S2) or 10-14h (184v HMEC) post plating using either 160 KV X-ray or ^{60}Co γ-radiation with a total dose of 2Gy. Control plates were sham irradiated. In some experiments, medium was supplemented with 10μg/ml TGFβ pan-specific neutralizing antibody (R&D Systems, Minneapolis, MN) or with an equivalent concentration of non-specific mouse IgG. When noted, some cultures were treated with 10μm U0126 (Cell Signaling, Beverly, MA) or DMSO.

Reagents: Antibodies to phosphorylated Erk1/2 (Thr202/Tyr204), phosphorylated MEK (Ser217/221), Erk1/2 and Mek1/2 were from Cell Signaling. Phalloidin was from Molecular Probes (Eugene, OR). E-cadherin, β-catenin and N-cadherin antibodies were purchased from BD Biosciences (San Jose, CA) and vimentin-clone VIM 13.2, β-actin and fibronectin antibodies were from Sigma (St. Louis, MO). ZO-1 antibody was obtained from Zymed (South San Francisco, CA). SMAD 2/3 antibody was purchased from Santa Cruz Biotechnology (Santa Cruz, CA). Recombinant TGFβ1 and TGFβ pan-specific neutralizing antibody were obtained from R&D Systems.

Immunofluorescence: Cells grown on LabTek 8-well chamber slides; fixed with 80% methanol for 10 min (N-cadherin, ZO-1) or methanol:acetone (vimentin, β-catenin) or 4% paraformaldehyde (fibronectin, SMAD3, phalloidin) followed by treatment with 0.1% Triton (N-cadherin, SMAD3) for 10 min. For E-cadherin staining cells were either fixed with 80% methanol or extracted with CSK buffer (15), followed by 4% paraformaldehyde fixation. Nuclei were counterstained with DAPI (4',6-Diamidino-2-Phenylindole) using 0.5 ng/ml.

TGFβ Bioassay: Mink lung cells transfected with the promoter of plasminogen activator inhibitor linked to a luciferase reporter (PAI-L) were used to analyze TGFβ in the conditioned media as previously reported (18).

Protein analysis: Cells were lysed as previously described (15) or a in buffer containing 50 mM Tris-HCl, pH 7.5, 150 mM NaCl, 0.5 mM $MgCl_2$, 0.2 mM EGTA, 1% Triton X-100, protease inhibitor mixture (20 μl/ml; Sigma), 1 mM Pefabloc and 50mM glycerol-2-phosphate (Sigma) or phosphatase inhibitor cocktail set II (Calbiochem, San Diego, CA). Extraction and immunoprecipitation of soluble and insoluble pools of E-cadherin was done as previously described (19). Proteins were separated on 4-15% SDS-PAGE gels and transferred to Immobilon-P (Millipore, Billerica, MA) or nitrocellulose (Amersham Lifescience); and probed with indicated primary antibodies. In some instances, detection was accomplished using chemiluminescence of secondary antibodies labeled with horseradish peroxidase followed by densitometry analysis of films. Alternatively, detection was performed using the Odyssey system (LI-COR, Lincoln, NE) as previously described (20). Target proteins were normalized to β-actin for loading.

Motility and invasion assays: Confluent HMT3522 S1 or MCF10A cultures were grown in medium containing EGF. The cultures were scratched with a pipette tip and washed to

remove detached cells. The invasion assay was performed as previously described (21). The number of invading cells was the average of 3 wells from 2 duplicate experiments.

RNA purification: Cells were washed with PBS; denatured in Trizol; scrapped and subjected to chloroform extraction. After centrifugation, the upper phase was precipitated with an equal volume of isopropanol. RNA precipitates were resuspended in RNase free water and further purified on RNeasy columns (Qiagen, Germany). RNA quality was assessed on an Agilent Bio-Analyzer. The dataset analyzed by microarray included biological duplicates for each treatment in two independent experiments and three sham-treated samples.

Microarray processing and analysis: Cy3/Cy5-labeled cDNAs were generated from RNA and hybridized to HG-U133A chips (Affymetrix Inc.,) at the Lawrence Berkeley National Laboratory HTArray Core Facility (http://hta.lbl.gov). Samples were analyzed and clustered with the (UNO) One Color Genetraffic^{TM} software version 3.2-12 (Iobion Informatics LLC, Stratagene, La Jolla, CA). Genes whose expression was specifically altered by treatment were defined as those in which Cy5/Cy3 ratio was more than 1.75 fold ($|\text{mean log2ratio}|>0.8$) from baseline in at least three out of the four treated samples compared to the three sham samples. Significance analysis tests ($p<0.05$) were performed using Excel between sham samples and either IR, TGFβ or TGFβ+IR samples.

Real-time polymerase chain reaction (PCR): Total RNAs were pre-treated with amplification grade DNAse I (Invitrogen, Carlsbad, CA) then primed with random hexamers to generate cDNAs using a Superscript^{TM} III first-strand synthesis kit according to the manufacturer's intructions (Invitrogen). 1µl of non diluted cDNAs were then amplified with Lightcycler FastStart DNA master SYBR Green I (Roche Applied Science, Mannheim, Germany) using a Light Cycler (Roche Applied Science, Mannheim, Germany). TCF8, FGF2 and CDH1 specific primers optimized for SYBR Green real-time PCR were purchased from SuperArray Bioscience Corporation (Frederick, MD).

Image acquisition, processing and analysis: Imaging was done as previously described (20). Colony segmentation from phase images was done using live wire tool from MIPAV (22). Area and shape factors were calculated using Matlab (MathWorks Inc, Natick, MA) and DIPimage (image processing toolbox for Matlab, Delft University of Technology, The Netherlands).

Results

The progeny of irradiated HMEC undergo EMT in response to TGFβ

We previously reported that E-cadherin immunofluorescence significantly decreased in double-treated HMT3522 S1 cultured in Matrigel compared to control or single-treated cells and failed to establish acinar morphology typical of HMEC (9). EMT is one means of disrupting morphogenesis, e.g. during wound healing. To examine the possibility that EMT underlies the response to radiation and TGFβ, we compared the epithelial characteristics of HMEC in traditional monolayer culture. HMEC were irradiated with 2 Gy shortly after attachment, or treated with low concentrations of TGFβ (400 pg/ml), or double-treated, and cultured to approximately 80% confluence. As observed previously, E-cadherin and β-catenin immunolocalization in monolayer HMEC was significantly reduced in double-treated cells (Figure 1A). The function of an epithelium as a barrier requires the establishment of tight junctions, evident by lateral, apical localization of ZO-1. ZO-1 immunofluorescence showed distinct punctate localization at cell borders of control and irradiated cells. TGFβ treatment somewhat altered ZO-1 staining, such that it appeared as a coarser, punctate-like pattern at the cell boundaries (Figure 1A). However, ZO-1 staining completely disappeared in double-treated cells.

Notably, double treatment resulted in spindle shaped, elongated cells, a phenotype which was examined by phalloidin staining of actin. Actin localized mainly at cell-cell borders of control and irradiated HMEC with very few stress fibers. TGFβ alone elicited a mild change in actin organization. Double-treated cells displayed dramatic actin reorganization consisting of longitudinal stress fibers, characteristic of fibroblasts (Figure 1A).

In light of the loss of epithelial markers in irradiated HMEC cultured with TGFβ, we investigated whether there was a concomitant gain of mesenchymal markers, fibronectin, vimentin and N-cadherin (Figure 1B). Immunofluorescence analysis of the double-treated group revealed increased fibronectin deposition compared to sham and single-treated cells. Accumulated fibronectin was arrayed perpendicular to the cell edge and in randomly oriented networks. The intermediate filament protein vimentin dramatically increased following double treatment. Consistent with the shift to an elongated morphology, vimentin filaments were organized in a longitudinal meshwork. N-cadherin is normally present mainly in neuronal and muscle tissues, but is aberrantly expressed in epithelial tumors where it has been proposed to promote migration and invasiveness of carcinoma cells (23). N-cadherin immunofluorescence was dramatic increased following double treatment in a pattern reciprocal to E-cadherin loss.

Loss of epithelial markers and gain of mesenchymal markers in double-treated cells was accompanied by epithelial to mesenchymal cell shape change. Phase microscopy HMT3522 S1, MCF10A and 184v HMEC (Figure 1C) showed that untreated HMEC and irradiated cells displayed typical cuboidal appearance of epithelial cells. TGFβ elicited a modest shape change, particularly in 184v HMEC. In contrast, the morphology of all three HMEC following double-treatment shifted to spindle-shaped. The morphological response was observed even when TGFβ was added 48h post-IR, and was not reversible upon removal of TGFβ from the culture media for 48h (data not shown). Taken together, the concomitant increased expression of mesenchymal markers, loss of epithelial markers

and morphological response of the progeny of irradiated HMEC to TGFβ suggest that cells have undergone EMT.

TGFβ alters the cytoskeletal associated E-cadherin/β-catenin complexes in irradiated HMEC

Although E-cadherin immunofluorescence was significantly reduced only in double-treated cells (Figure 1A), western blot analysis of total E-cadherin protein expression levels were comparable in TGFβ-treated and double-treated groups (Figure 2A). β-catenin protein levels followed the same pattern. This observation suggested that immunofluorescence was a function of protein localization, rather than abundance. In epithelial cells, E-cadherin and β-catenin are associated with the cytoskeleton at intercellular junctions that are resistant to detergent extraction (24). We tested whether the difference between immunofluorescence and immunoblotting was due to solubility by using differential detergent extraction followed by E-cadherin immunoprecipitation. Although TGFβ reduced the soluble pool of E-cadherin regardless of irradiation, the insoluble, cytoskeletal associated E-cadherin was significantly decreased only in double-treated cells (Figure 2B). The distribution of β-catenin was similarly affected. Thus, TGFβ alters the cytoskeletal associated E-cadherin/β-catenin complexes only in irradiated HMEC.

Functional consequence of the response of irradiated HMEC to TGFβ

During physiological processes and in cancer, EMT is often accompanied by acquisition of cell motility and invasiveness (11). We analyzed the migratory properties of double-treated HMEC using a monolayer scratch assay and time-lapse videomicroscopy (Figure 3A). Control or irradiated cells moved as a sheet evidenced by a smooth edge and failed to fill the gap during the 40h observation period. Consistent with their intermediate cytoskeletal and cell-cell adhesion phenotype, TGFβ-treated HMEC began to close the wound after 20h, but the cells still maintained sheet formation and by 40h had not closed the gap. In contrast, irradiated HMEC cultured with TGFβ moved as single, spindle-shaped cells and closed the gap by 40h by forming multicellular bridges of spindle shaped cells between the two areas. Thus the tissue-specific requirement for epithelia to maintain cell interactions as a sheet of cohesive cells is disrupted when irradiated HMEC are exposed to TGFβ, which leads to independent single cell migration characteristic of mesenchymal cells.

The above observations led us to further investigate the invasive properties of HMEC by invasion assay through a membrane coated with Matrigel™, a basement membrane type matrix. HMT 3522 S1 did not invade in this assay under any condition. Therefore we used HMT 3522 S2, which are derived from further propagation of HMT 3522 S1 in EGF-free media (21). Cells were cultured as described above, then trypsinized and plated into the Boyden chamber assay in standard media. Few control HMT 3522 S2 cells were able to invade. The progeny of irradiated cells demonstrated greater invasion than treatment with TGFβ alone when compared to the control. In contrast, irradiation of S2 cells and subsequent culture in the presence of TGFβ increased the number of invading cells more than 100-fold compared to sham (Figure 3B).

There is ongoing discussion in the literature as to what criteria define true EMT *in vitro* and how to distinguish the EMT phenotype from a 'scattering' phenotype (11). Both phenotypes exhibit disruption of cell junctions, fibroblast-type morphology, and enhanced motility. However, it has been suggested that they can be distinguished by reversibility since the EMT phenotype, but not the scattering phenotype, persists after withdrawal of the stimulus (11). As mentioned above, TGFβ withdrawal did not reverse the morphological shift, consistent with EMT. Since the progeny of irradiated HMEC cultured with TGFβ exhibit disrupted morphogenesis in Matrigel™ (9), we used morphogenesis as a stringent test of persistence. Single and double-treated HMEC cells were trypsinized and replated in Matrigel™ for analysis of acinar morphogenesis without further TGFβ stimulation. Replated double-treated cells formed larger colonies than control or single treated cells, which was measured by increased size and irregularity of colony shape (Figure 3C). We concluded that the phenotype elicited by IR and TGFβ resulting in dysplastic morphogenesis (i.e. 3D growth deregulation and disorganization) and the persistence of these morphological alterations in the absence of additional TGFβ is further evidence of EMT.

Irradiated HMEC produce active TGFβ

Latent TGFβ is activated in the irradiated mouse mammary gland *in vivo* (6), which could increase the susceptibility of irradiated cells to undergo TGFβ mediated EMT by decreasing a threshold response. Nuclear translocation of receptor phosphorylated SMAD2 or 3 (R-SMAD) results from liganded TGFβ receptor (8). Immunofluorescence analysis demonstrated that R-SMAD nuclear localization increased by 30% in irradiated HMEC 6 days after irradiation compared to control cells (Figure 4A). These data suggest that IR elicits persistent TGFβ signaling. To determine whether IR increased TGFβ production or activation, we analyzed the conditioned medium (CM) from irradiated cells using a TGFβ bioassay (18). Bioassay of irradiated and control HMEC CM indicated similar levels of latent TGFβ. Active TGFβ, however, was undetectable in either CM (data not shown). Since the sensitivity of detection in CM for the bioassay is approximately 0.2 ng/ml, we reasoned that low levels of TGFβ could be functional, although undetectable by bioassay. If so, then the CM should give rise to a similar phenotype in unirradiated HMEC seen in response to addition of exogenous TGFβ. To investigate this hypothesis, we fed non-irradiated HMEC with 50% CM from either irradiated or non-irradiated HMEC cultures. CM from irradiated cells caused a significant decrease in E-cadherin protein levels when compared to cells treated with CM from non-irradiated cells. This response was reversed by adding TGFβ neutralizing antibody to the cells grown in the presence of IR-treated CM (Figure 4B). To confirm that this biological activity produced by irradiated cells was indeed TGFβ, irradiated cells were grown in the absence or presence of TGFβ neutralizing antibody. When irradiated HMEC were grown in the presence of TGFβ neutralizing antibody there was a significant reversal of the decrease in E-cadherin protein abundance compared to cells grown with control IgG control antibody (Figure 4C).

Based on the above data, we estimated that irradiated cultures produce approximately 100 pg/ml of active TGFβ. We then tested whether EMT was a function of the additive effect

of exogenous (400 pg/ml) and endogenous TGFβ (approximately 100 pg/ml) by treating HMEC with graded concentrations of TGFβ. However, MCF10A treated with up to 1200 pg/ml TGFβ did not undergo EMT (data not shown). Although IR induced TGFβ activity in cultured HMEC, as it did in the mouse mammary gland (6), it was insufficient to disrupt HMEC acinar morphogenesis as shown in our previous study (9). Moreover, the progeny of irradiated HMT 3522 S1, MCF10A and 184v HMEC exhibited a modest response in terms of epithelial morphology, E-cadherin expression or invasion. Thus, chronic TGFβ activation by irradiated HMEC is insufficient to drive the EMT phenotype.

Genetic programs underlying EMT in double-treated HMEC

In order to comprehensively describe the altered epithelial cell phenotype following double treatment, we compared transcript expression levels in sham, IR-, TGFβ- and double-treated HMEC. The expression profile of the progeny of irradiated HMEC was similar to control HMEC. 43 genes were differentially expressed by TGFβ-treated HMEC that included 28 up-regulated genes and 15 down-regulated genes with a >1.75-fold change in expression compared to sham samples (Supplementary Table). We identified 10 genes that constituted the double-treatment signature. Expression was significantly increased for five genes and decreased for the five other genes after double treatment compared to TGFβ alone.

The five significantly up-regulated genes in double-treated samples were the growth factor FGF2/bFGF, the serine/cysteine proteinase inhibitor, SERPINA1, the interleukin 1 receptor-like protein, IL1RL1, the transcription factor TCF8/ZEB-1 and the zinc transporter SLC39A8 (Figure 5A and B). The five down-regulated genes in double-treated HMEC were the Wnt pathway transcription repressor secreted frizzle related protein 1 (SFRP1), the cystein-rich protein, CRIP2, the aldo-keto reductase, AKR1C2, the cadherin EGF LAG seven-pass G-type receptor 2 (CELSR2), and the aminopeptidase O, C9orf3. Although transcript levels of five of these ten genes (SERPINA1, SLC39A8, CRIP2, AKR1C2 and CELSR2) were higher in TGFβ-treated samples than in sham samples, they were below the 1.75-fold cut off used to define TGFβ-responsive genes. Changes in gene expression in double-treated HMEC were validated for TCF8 and FGF2, by real-time RT-PCR (Figure 5B). For comparison, real-time RT-PCR of E-cadherin (CDH1) was decreased in both TGFβ and double treated cells, consistent with the protein levels shown in Figure 2A.

The EMT signature genes have roles in cell-matrix interactions, cell motility/invasion, inflammation and disruption of adherens junctions. The products of TCF8/ZEB1 and FGF2 have been described to repress E-cadherin transcription and to promote EMT (25, 26). Some of the TGFβ-responsive and EMT-associated signatures genes identified here have been previously described (27, 28). An extensive bibliography search showed that 5 of the 10 EMT signature genes are directly or indirectly associated with the Erk/MAPK pathway, suggesting a specific functional role of Erk/MAPK activation in inducing EMT upon double-treatment. Several reports suggest that an independent stimulus must synergistically proceed or at least accompany the induction of EMT. The multiple

downstream effectors of Ras, such as MAPK, may be a requirement to induce a pre-malignant state and endow epithelial cells with an increased rate of proliferation (29).

Persistent activation of Erk/MAPK in double-treated HMEC

Consequently, we examined the possible involvement of the Erk/MAPK signaling cascade in the mediation of TGFβ-induced EMT in irradiated HMEC by determining the activation of Erk1/2 and upstream activators, Mek1/2. The total amounts of Erk or Mek were similar following all treatments. Phosphorylated-Erk1/2 was modestly induced by TGFβ but was significantly increased in irradiated HMEC treated with TGFβ (Figure 6A, top panel). Consistent with this, Mek1/2 activation, as indicated by phosphorylation, was also increased upon double treatment.

There is a significant body of literature that suggests that Erk activation is required to initiate the EMT program (30, 31). IR can induce a rapid, ligand-independent activation of Erk/MAPK in cancer cells (32). To investigate whether activation of Erk1/2 by IR or TGFβ *versus* double treatment was indeed instrumental in driving EMT, we monitored Mek/Erk activation at early time points (4-48h post IR). At 8h, Erk1/2 phosphorylation was significantly induced by IR when compared to TGFβ or double-treatment. From 12-24h, MAPK pathway activation increased following IR or TGFβ or double treatment compared to controls. However, at 48h post-IR, double-treated cells exhibited greater Erk activation compared to control and to single-treated HMEC (Figure 6, bottom panel).

To determine if persistent Erk activation was required for the EMT phenotype in double-treated HMEC, we used U0126, a specific Mek small molecule inhibitor. Treatment with U0126 dramatically decreased Erk activation in HMEC (Figure 6B). Treatment with U0126 also restored E-cadherin and cytoskeletal rearrangement (Figure 6C) and reduced cell migration in the wound closure assay (Figure 6D). These data suggest that IR and TGFβ collaborate to increase Erk activation, which is necessary for establishment and maintenance of EMT (7 days). We propose that transient IR-induced Erk activation is sustained in the presence of additional TGFβ, and that this event predisposes non-malignant HMEC to undergo TGFβ-mediated EMT.

Discussion

Here we report that the progeny of irradiated HMEC are dramatically sensitized to undergo TGFβ-induced EMT. IR and TGFβ cooperated to induce a phenotypic transition that occurred in the progeny of cells irradiated once and persisted even in the absence of TGFβ. This resulted in increased motility, enhanced invasion, disrupted epithelial morphogenesis, and was accompanied by a distinct pattern of gene expression.

TGFβ has long been considered as both a positive and a negative effector of mammary tumorigenesis, acting early as a tumor suppressor but later as a stimulator of tumor invasion (8). Overexpression of constitutively active TGFβ can induce EMT during tumor progression *in vivo* (33) and the overexpression of TGFβ has been associated with poor prognosis of many human cancers (8). The phenotypes of breast cancer micrometastases in lymph nodes and the bone marrow have been interpreted as evidence that EMT occurs in primary tumors (34). However *in vivo* verification of EMT has been controversial, perhaps due to the transient and reversible nature of the process and to the lack of analytical tools that distinguish carcinoma cells undergoing EMT from neighboring stromal fibroblasts.

In vitro studies of EMT were originally described in cells of murine origin, frequently containing *ras* mutations. It has been reported in a very limited number of human cell lines, and very rarely in non-malignant cell lines (35, 36). The *in vitro* studies in which TGFβ alone is capable of inducing EMT have either been performed in serum containing medium, which provides various growth factors commonly associated with wounding, including TGFβ, FGF and EGF, and/or using high TGFβ concentrations (2.5-10ng/ml) (36, 37). Expression profiling of genetic program underlying EMT of HaCat keratinocytes stimulated with TGFβ to undergo EMT identified 80 EMT-related targets (27). Our expression profiling study distinguishes between genes regulated by TGFβ without concomitant EMT in non-malignant HMEC and genes that are differentially expressed under conditions resulting in EMT.

We identified 10 genes specifically associated with EMT, five of which were not induced at all by TGFβ alone. Transcriptional repression of E-cadherin, could be mediated by the transcription factor TCF8/ZEB1 (25). FGF2, whose transcript expression is significantly increased upon double treatment in this EMT model, has also been linked to E-cadherin repression and EMT (25, 26). Low E-cadherin immunoreactivity in breast cancer is associated with poor prognosis (38), whereas restoration of E-cadherin reverts the invasive phenotype of cancer cells (39). Irradiated HMEC redistribute E-cadherin from an insoluble to a soluble pool when cultured with TGFβ, which is accompanied by a significant increase in N-cadherin. The cadherin switch from E- to N-cadherin frequently accompanies pronounced tissue reorganization in normal and pathological conditions (40). Studies on cancer cell lines indicate that N-cadherin is linked to a more malignant and invasive behavior (23). Consistent with this, double-treated HMEC were significantly more motile. Although double-treated HMT-3522 S1 cells were not invasive, double-treatment induced invasive behavior in HMT-3522 S2 cells, which are an EGF-independent strain of the HMT-3522 progression series.

Neither chronic TGFβ signaling induced by irradiation nor supplementation with low TGFβ concentrations was sufficient to induce the EMT phenotype in any of the three HMEC that were examined in our studies. EMT occurred only in irradiated HMEC in the presence of TGFβ, even when TGFβ was added 2 days post-IR. This suggested that a IR-induced event was a prerequisite for TGFβ-mediated EMT that was sustained for 48h. IR initially induces a transient activation of Erk/MAPK *via* a ligand-independent mechanism (32). Although the involvement of Erk signaling in TGFβ–induced EMT is controversial (41), many studies have shown a requirement for overexpression/mutational activation of elements of the Ras/Raf/Erk pathway for TGFβ–mediated EMT (41-43). Furthermore, the importance of enhanced Erk activation in induction of EMT is also supported by studies in which Erk activity induced by Ras/TGFβ (41), EGF/TGFβ (31), HGF/ErB2 (44) and Akt (45), was found to be critically involved in EMT. Our data suggest a model in which IR-induced Erk/MAPK signaling is sustained by TGFβ, is required for establishing and maintaining EMT, and is essential for the functional response, i.e. enhanced migration.

Cancer radiotherapy is primarily limited in many organs by the risk of developing fibrosis (46). Neilson and colleagues demonstrated EMT as a significant source of fibrosis in a kidney ligation model (47). An interesting implication from our study is that normal epithelia may undergo EMT in response to irradiation and TGFβ, which could contribute to fibrosis following radiotherapy. If so, this would lend further credence to the potential application of TGFβ inhibitors in radiotherapy.

Based on studies in mouse mammary gland, we proposed that the action of radiation as a carcinogen is augmented by its ability to modulate signaling from the microenvironment (48). Tumorigenesis is increased 4-fold when unirradiated preneoplastic mammary epithelial cells are transplanted to the mammary stroma of a host irradiated with 4 Gy (3). IR induces abundant TGFβ activation (6). Our current and earlier studies (9) have shown that irradiated non-malignant HMEC undergo EMT only if they are exposed to additional TGFβ, as might be derived from the stroma in intact tissues. If moderate radiation doses can prime preneoplastic cells to undergo EMT, it could accelerate cancer progression. Interestingly, a recent study shows that conventional renal cell carcinomas of the Ukrainian patients living in the radio-contaminated areas exhibited significantly higher levels of TGFβ expression compared to similar tumors in populations in uncontaminated areas (49). These tumors were characterized by decreased or abnormal distribution of fibronectin, laminin, and E-cadherin/βcatenin, suggesting that chronic low level radiation exposure in humans might indeed shift tumors towards a mesenchymal phenotype. Nonetheless there is little evidence to support these events occurring in normal epithelia *in vivo* after moderate doses. Furthermore, additional studies from our laboratory indicate that TGFβ is instrumental in mounting a DNA damage response (7, 20), and in inducing apoptosis of genomically unstable cells (Barcellos-Hoff, M.H. and Maxwell, C.A. unpublished observations). The complexity of radiation effects mediated by TGFβ will require further study to determine whether it plays a proximal role in suppressing or promoting radiogenic carcinogenesis.

Acknowledgments

We thank Samuel Haile, Megha Gupta, James Chen, Haleh Sakkaki, Jeremy Semeiks and Howard Park for their experimental assistance.

References

1. Barcellos-Hoff MH. It takes a tissue to make a tumor: Epigenetics, cancer and the microenvironment. J Mammary Gland Biol Neoplasia 2001;6:213-21.
2. Kenny PA, Bissell MJ. Tumor reversion: correction of malignant behavior by microenvironmental cues. Int J Cancer 2003 Dec 10;107(5):688-95.
3. Barcellos-Hoff MH, Ravani SA. Irradiated mammary gland stroma promotes the expression of tumorigenic potential by unirradiated epithelial cells. Cancer Res 2000;60:1254-60.
4. Dent P, Yacoub A, Contessa J*, et al.* Stress and radiation-induced activation of multiple intracellular signaling pathways. Radiat Res 2003;159(3):283-300.
5. Barcellos-Hoff MH, Park C, Wright EG. Radiation and the microenvironment - tumorigenesis and therapy. Nat Rev Cancer 2005 Nov;5(11):867-75.
6. Barcellos-Hoff MH. Radiation-induced transforming growth factor β and subsequent extracellular matrix reorganization in murine mammary gland. Cancer Res 1993;53:3880-6.
7. Ewan KB, Henshall-Powell RL, Ravani SA*, et al.* Transforming Growth Factor-β1 Mediates Cellular Response to DNA Damage in Situ. Cancer Res 2002 October 15, 2002;62(20):5627-31.
8. Bierie B, Moses HL. Tumour microenvironment: TGFbeta: the molecular Jekyll and Hyde of cancer. Nat Rev Cancer 2006 Jul;6(7):506-20.
9. Park CC, Henshall-Powell R, Erickson AC*, et al.* Ionizing Radiation Induces Heritable Disruption of Epithelial Cell-Microenvironment Interactions. Proc Natl Acad Sci 2003;100(19):10728-33.
10. Cui W, Fowlis DJ, Bryson S*, et al.* TGFβ1 inhibits the formation of benign skin tumors, but enhances progression to invasive spindle carcinomas in transgenic mice. Cell 1996;86(4):531-42.
11. Grunert S, Jechlinger M, Beug H. Diverse cellular and molecular mechanisms contribute to epithelial plasticity and metastasis. Nat Rev Mol Cell Biol 2003;4(8):657-65.
12. Petersen OW, Nielsen HL, Gudjonsson T*, et al.* Epithelial to mesenchymal transition in human breast cancer can provide a nonmalignant stroma. Am J Pathol 2003 Feb;162(2):391-402.
13. Moody SE, Perez D, Pan TC*, et al.* The transcriptional repressor Snail promotes mammary tumor recurrence. Cancer Cell 2005 Sep;8(3):197-209.
14. Brown KA, Aakre ME, Gorska AE*, et al.* Induction by transforming growth factor-beta1 of epithelial to mesenchymal transition is a rare event in vitro. Breast Cancer Res 2004;6(3):R215-31.
15. Weaver VM, Petersen OW, Wang F*, et al.* Reversion of the malignant phenotype of human breast cells in three-dimensional culture and in vivo by integrin blocking antibodies. J Cell Biol 1997;137(1):231-45.
16. Stampfer MR. Isolation and growth of human mammary epithelial cells. J Tissue Culture Met 1985;9(2):107-15.
17. Madsen MW, Lykkesfeldt AE, Laursen I, Nielson KV, Briand P. Altered gene expression of c-myc, epidermal growth receptor, transforming growth factor alpha, and c-

erb-B2 in an immortalized human breast epithelial cell line, HMT-3522, is associated with decreased growth factor requirements. Cancer Res 1992;52:1210-7.
18. Abe M, Harpel JG, Metz CN, Nunes I, Loskutoff DJ, Rifkin DB. An assay for transforming growth factor-beta using cells transfected with a plasminogen activator inhibitor-1 promoter-luciferase construct. Analyt Biochem 1994;216(2):276-84.
19. Hinck L, Nathke IS, Papkoff J, Nelson WJ. Dynamics of cadherin/catenin complex formation: novel protein interactions and pathways of complex assembly. J Cell Biol 1994 Jun;125(6):1327-40.
20. Kirshner J, Jobling MF, Pajares MJ*, et al.* Inhibition of TGFβ1 Signaling Attenuates ATM Activity in Response to Genotoxic Stress. Cancer Res 2006;66(22):10861-68.
21. Lochter A, Srebrow A, Sympson CJ, Terracio N, Werb Z, Bissell MJ. Misregulation of stromelysin-1 expression in mouse mammary tumor cells accompanies acquisition of stromelysin-1-dependent invasive properties. J Biol Chem 1997;272(8):5007-15.
22. McAuliffe M, Lalonde F, McGarry D, Gandler W, Csaky K, BLTrus. Medical Image Processing, Analysis & Visualization In Clinical Research. IEEE: COMPUTER-BASED MEDICAL SYSTEMS (CBMS) 2001:381-6.
23. Nieman MT, Prudoff RS, Johnson KR, Wheelock MJ. N-Cadherin Promotes Motility in Human Breast Cancer Cells Regardless of their E-Cadherin Expression. J Cell Biol 1999 November 1, 1999;147(3):631-44.
24. Conacci-Sorrell M, Zhurinsky J, Ben-Ze'ev A. The cadherin-catenin adhesion system in signaling and cancer. J Clin Invest 2002 April 15, 2002;109(8):987-91.
25. Chua HL, Bhat-Nakshatri P, Clare SE, Morimiya A, Badve S, Nakshatri H. NF-kappaB represses E-cadherin expression and enhances epithelial to mesenchymal transition of mammary epithelial cells: potential involvement of ZEB-1 and ZEB-2. Oncogene 2006 Jul 24.
26. Strutz F, Zeisberg M, Ziyadeh FN*, et al.* Role of basic fibroblast growth factor-2 in epithelial-mesenchymal transformation. Kidney Int 2002;61(5):1714-28.
27. Zavadil J, Bitzer M, Liang D*, et al.* Genetic programs of epithelial cell plasticity directed by transforming growth factor-beta. Proceedings of the National Academy of Sciences of the United States of America 2001 Jun;98(12):6686-91.
28. Xie L, Law BK, Aakre ME*, et al.* Transforming growth factor beta-regulated gene expression in a mouse mammary gland epithelial cell line. Breast Cancer Res 2003;5(6):R187-98.
29. Gotzmann J, Mikula M, Eger A*, et al.* Molecular aspects of epithelial cell plasticity: implications for local tumor invasion and metastasis. Mutat Res 2004;566(1):9-20.
30. Xie L, Law BK, Chytil AM, Brown KA, Aakre ME, Moses HL. Activation of the Erk pathway is required for TGF-beta1-induced EMT in vitro. Neoplasia 2004 Sep-Oct;6(5):603-10.
31. Grande M, Franzen A, Karlsson JO, Ericson LE, Heldin NE, Nilsson M. Transforming growth factor-beta and epidermal growth factor synergistically stimulate epithelial to mesenchymal transition (EMT) through a MEK-dependent mechanism in primary cultured pig thyrocytes. J Cell Sci 2002 Nov 15;115(Pt 22):4227-36.

32. Schmidt-Ullrich RK, Mikkelsen RB, Dent P*, et al.* Radiation-induced proliferation of the human A431 squamous carcinoma cells is dependent on EGFR tyrosine phosphorylation. Oncogene 1997 Sep 4;15(10):1191-7.
33. Portella G, Cumming SA, Liddell J*, et al.* Transforming growth factor beta is essential for spindle cell conversion of mouse skin carcinoma in vivo: implications for tumor invasion. Cell Growth Differ 1998;9:393-404.
34. Braun S, Pantel K. Biological characteristics of micrometastatic cancer cells in bone marrow. Cancer Metastasis Rev 1999;18(1):75-90.
35. Seton-Rogers SE, Lu Y, Hines LM*, et al.* Cooperation of the ErbB2 receptor and transforming growth factor beta in induction of migration and invasion in mammary epithelial cells. Proc Natl Acad Sci U S A 2004 Feb 3;101(5):1257-62.
36. Valcourt U, Kowanetz M, Niimi H, Heldin CH, Moustakas A. TGF-beta and the Smad signaling pathway support transcriptomic reprogramming during epithelial-mesenchymal cell transition. Mol Biol Cell 2005 Apr;16(4):1987-2002.
37. Miettinen PJ, Ebner R, Lopez AR, Derynck R. TGF-β induced transdifferentiation of mammary epithelial cells to mesenchymal cells: involvement of type I receptors. J Cell Biol 1994;127:2021-36.
38. Heimann R, Lan F, McBride R, Hellman S. Separating favorable from unfavorable prognostic markers in breast cancer: the role of E-cadherin. Cancer Res 2000 2000 Jan 15;60(2):298-304.
39. Vleminckx K, Vakaet LJ, Mareel M, Fiers W, van Roy F. Genetic manipulation of E-cadherin expression by epithelial tumor cells reveals an invasion suppressor role. Cell 1991 1991 Jul 12;66(1):107-19.
40. Cavallaro U, Schaffhauser B, Christofori G. Cadherins and the tumour progression: is it all in a switch? Cancer Lett 2002 Feb 25;176(2):123-8.
41. Janda E, Lehmann K, Killisch I*, et al.* Ras and TGF{beta} cooperatively regulate epithelial cell plasticity and metastasis: dissection of Ras signaling pathways. J Cell Biol 2002 January 21, 2002;156(2):299-314.
42. Oft M, Akhurst RJ, Balmain A. Metastasis is driven by sequential elevation of H-ras and Smad2 levels. Nat Cell Biol 2002 Jul;4(7):487-94.
43. Gotzmann J, Huber H, Thallinger C*, et al.* Hepatocytes convert to a fibroblastoid phenotype through the cooperation of TGF-beta1 and Ha-Ras: steps towards invasiveness. J Cell Sci 2002 Mar 15;115(Pt 6):1189-202.
44. Khoury HJ, Loberiza FR, Jr., Ringden O*, et al.* Impact of posttransplantation G-CSF on outcomes of allogeneic hematopoietic stem cell transplantation. Blood 2006 Feb 15;107(4):1712-6.
45. Irie HY, Pearline RV, Grueneberg D*, et al.* Distinct roles of Akt1 and Akt2 in regulating cell migration and epithelial-mesenchymal transition. J Cell Biol 2005 Dec 19;171(6):1023-34.
46. Bentzen SM. Preventing or reducing late side effects of radiation therapy: radiobiology meets molecular pathology. Nat Rev Cancer 2006 Sep;6(9):702-13.
47. Iwano M, Fischer A, Okada H*, et al.* Conditional Abatement of Tissue Fibrosis Using Nucleoside Analogs to Selectively Corrupt DNA Replication in Transgenic Fibroblasts. Molecular Therapy 2001 2001/2;3(2):149-59.
48. Barcellos-Hoff MH. How do tissues respond to damage at the cellular level? The role of cytokines in irradiated tissues. Radiat Res 1998;150(5):S109-S20.

49. Romanenko A, Morell-Quadreny L, Ramos D, Nepomnyaschiy V, Vozianov A, Llombart-Bosch A. Extracellular matrix alterations in conventional renal cell carcinomas by tissue microarray profiling influenced by the persistent, long-term, low-dose ionizing radiation exposure in humans. Virchows Arch 2006 2006/03//:1-7.
50. Trujillo-Ortiz A, Hernandez-Walls R. MAOV1: Single-Factor Multivariate Anaysis of Variance test, http://www.mathworks.com/matlabcentral/fileexchange/loadFile.do?objectId=3863&objectType=FILE. 2003.

Figure Legends

Figure 1

Loss of epithelial and gain of mesenchymal markers in irradiated HMEC in response to TGFβ

(A) Immunolocalization of cytoskeleton-associated E-cadherin, β-catenin, ZO-1, F-actin (detected with phalloidin) (B) fibronectin, vimentin and N-cadherin in sham (untreated), IR, TGFβ and double-treated (IR+TGFβ) HMT3522 S1 cells. All images were acquired at 40x magnification. (C) Phase images of sham, IR, TGFβ and IR+TGFβ treated HMT3522 S1 (day 10), MCF10A (day 10) and 184v HMEC (day 7). The images were acquired at 10x magnification. All images in (A), (B) and (C) are representative of three independent experiments.

Figure 2

TGFβ alters the cytoskeletal associated E-cadherin/β-catenin complexes in irradiated HMEC

(A) Immunoblots and quantification of E-cadherin and β-catenin in total protein extracts from sham, IR, TGFβ or IR+ TGFβ HMT3522 S1 cultures. The graph represents quantification of E-cadherin protein abundance from nine independent experiments normalized to β-actin shown as mean±standard error. β-actin indicates equal protein loading. (B) Immunoblot of E-cadherin and β-catenin expression in E-cadherin immunoprecipitates from Triton soluble (S) and insoluble (I) protein extracts of HMT3522 S1 cells. (Student's t-test, p ** <0.0001)

Figure 3

TGFβ induces an increase in motility and invasiveness in irradiated HMEC.

(A) Wound closure assay in sham, IR, TGFβ and IR+ TGFβ treated HMT3522 S1 cells. Representative images captured with a 10x objective at the time of wounding (0h) and 20h or 40h after wounding. All experiments were repeated at least 3 times, with similar results. (B) Quantification of transwell migration assay using HMT3522 S2 cells. Values represent mean±SE of total cell counts of each well from duplicate experiments. (C) Further propagation of MCF10A in 3D matrix without additional treatment. Sham, IR or TGFβ-treated or double-treated MCF10A were grown to 80-90% confluency, trypsinized and embedded in Matrigel™ as previously described (9). Phase images of acini embedded in Matrigel™ were captured using 10x magnification. Acini were identified using the live wire tool from MIPAV and batch processed by in-house measurement routines (see material and method for details). Three separate experiments with multiple independent samples were analyzed. Averages of acini areas were plotted against their average shape factor for each sample. The shape factor is defined as $P^2/(4.\pi.A)$ where P is the perimeter and A the area of the acinus. This value is equal to one for a perfect circle. A value greater than 1 is interpreted as the amount of deformation in comparison to a circle. Averages of acini areas were plotted against their average shape factor for each sample.

A *p*-value of 1.8E-5 was obtained between sham and double treatment. All other groups could not be distinguished from sham. The circles on the scatterplot delimit the double-treated group compared to the other groups and indicates that double treatment leads to larger and more deformed acini. Statistical analysis of the 2D scatter plot between area and shape factor was performed by using multivariate analysis of variance (50).

Figure 4

Persistent effect of IR predisposes HMEC to TGFβ-induced EMT

(A) Immunolocalization and quantification of SMAD in sham and IR-treated HMT3522 S1 cultures at day 6 post plating. The graph represents quantification of nuclear SMAD positive cells from one of three experiments (mean± SD; sham n=5464 cells, IR n=4876 cells). (B) Quantification of E-cadherin protein abundance from three independent experiments normalized to β-actin is shown as mean±SE. HMT3522S1 cells were grown for 10 days in the presence of 50% CM from control (sham-CM) or irradiated (IR-CM) cells in presence of TGFβ neutralizing antibody or non specific IgG. (C) E-cadherin protein abundance in sham and IR-treated cells treated with TGFβ neutralizing antibody (TGFβ–NAb) or non specific IgG. Values are representative of 3 experiments normalized to β-actin shown as mean ± SE. (Student's t-test, p * <0.01; p ** <0.001; p *** <0.0001)

Figure 5

Gene expression profiles of double-treated HMEC.

(A) Microarray transcript profiling for 10 EMT signature genes (FGF2, SERPINA1, IL1RL1, TCF8, SLC39A8, SFRP1, CRIP2, AKR1C2, CELSR2 and C9orf3) in sham, IR-treated, TGFβ-treated and double-treated MCF10A cells 8 days post-IR. Biological replicates are shown. Although transcript levels of five of these ten genes (SERPINA1, SLC39A8, CRIP2, AKR1C2 and CELSR2) were significantly (<p, 0.05) higher in TGFβ-treated samples than in sham samples, alterations changes were all below the 1.75-fold cut off used to define TGFβ-responsive genes. The graph represents significance analysis of alterations in transcript expression levels (±SE) for the 10 EMT signature genes including the experiment shown in panel A and a replicate independent experiment (1 probe per gene except for FGF2 (2 probes) and SFRP1 (3 probes)), (B) Validation of microarray profiling for TCF8, FGF2 and CDH1 (E-cadherin) by real-time PCR. Increased TCF8 and FGF2 mRNA abundance is illustrated by a shift towards the left of the real time PCR curves in double-treated samples. CDH1 was decreased (right shifted curve) in TGFβ-treated and double-treated samples. (Student's t-test, p * <0.05; p ** <0.001; p *** <0.0001).

Figure 6

Kinetics of MAPK signaling in HMEC as a function of IR and TGFβ treatment.

(A) Erk and Mek activation in sham, IR, TGFβ and IR+TGFβ treated 184v HMEC. Sham, IR, TGFβ and IR+TGFβ treated cells were lysed 7 days (top panel) or 4-48h (bottom panel) post-IR, and immunoblotted with the indicated antibodies. Graphs represent densitometric analysis of immunoblots of phosphorylated Erk and/or Mek normalized to respective total protein. Error bars represent ± S.E. (B) At 6 days post-IR 184v HMEC were treated with DMSO or U0126 (10μM). 8h after treatment cells were lysed, and immunoblotted with the indicated antibodies. (C) Sham, IR, TGFβ and IR+TGFβ treated MCF10A cells (6 days post plating) were cultured in DMSO or U0126 (10μM) for 30h, followed by staining for F-actin (detected with phalloidin) and E-cadherin. Representative images of only IR+TGFβ treated cells are shown. E-cadherin and phalloidin images are representative of three and two independent experiments respectively. (D) Representative phase images of wound closure assay of sham, IR, TGFβ and IR+TGFβ in presence of DMSO or U0126 (10μM) at 0h and 14h. Images were acquired 14h after addition of DMSO or U0126. Phase images were captured using 4x objective. Three independent experiments were done and the graphs represent percentage of wound closure (±SD) at 14h after treatment from one such experiment.

Supplemental files

Two lists of up-regulated and down-regulated genes upon TGFβ treatment are provided. As described in the Methods section, TGFβ responsive genes are defined as genes for which at least three out of the four biological samples tested show a change of at least 1.75-fold compared to sham samples. In each list, genes are ranked from the most to the least responsive gene according to the averaged fold change in transcript level. The number of biological samples where the expression change is observed is indicated.

Figure 1

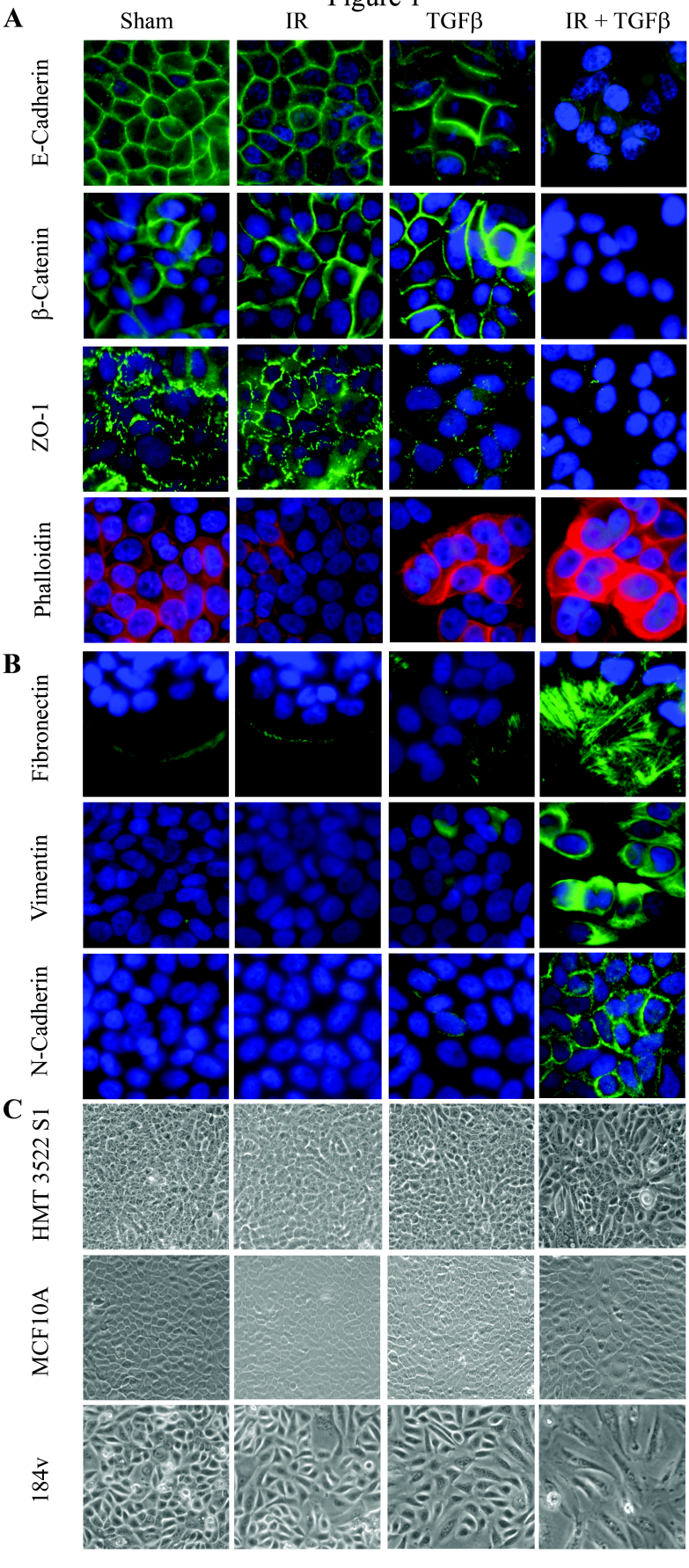
A
Sham
IR
TGFβ
IR + TGFβ
E-Cadherin
β-Catenin
ZO-1
Phalloidin
B
Fibronectin
Vimentin
N-Cadherin
C
HMT 3522 S1
MCF10A
184v

Figure 2

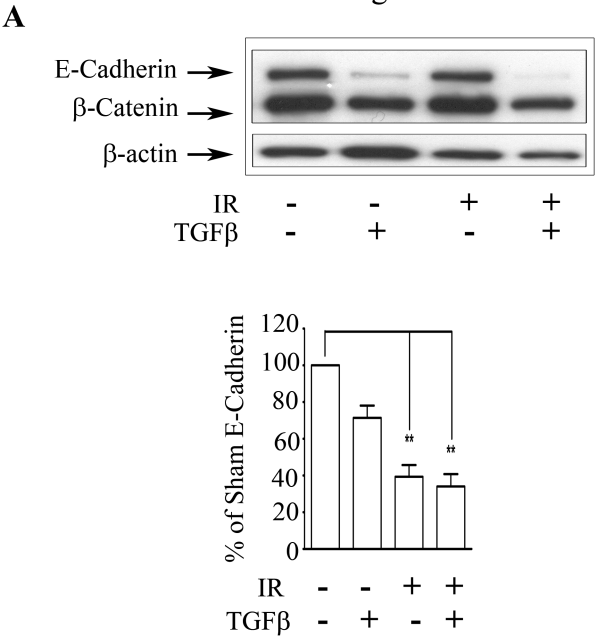
A
E-Cadherin
β-Catenin
β-actin
IR - - + +
TGFβ - + - +
% of Sham E-Cadherin
120
100
80
60
40
20
0
**
**
IR - - + +
TGFβ - + - +
B
IP: E-Cadherin
IB: E-Cadherin and β-Catenin
E-Cadherin
β-Catenin
S I S I S I S I
IR - - - - + + + +
TGFβ - - + + - - + +

Figure 3

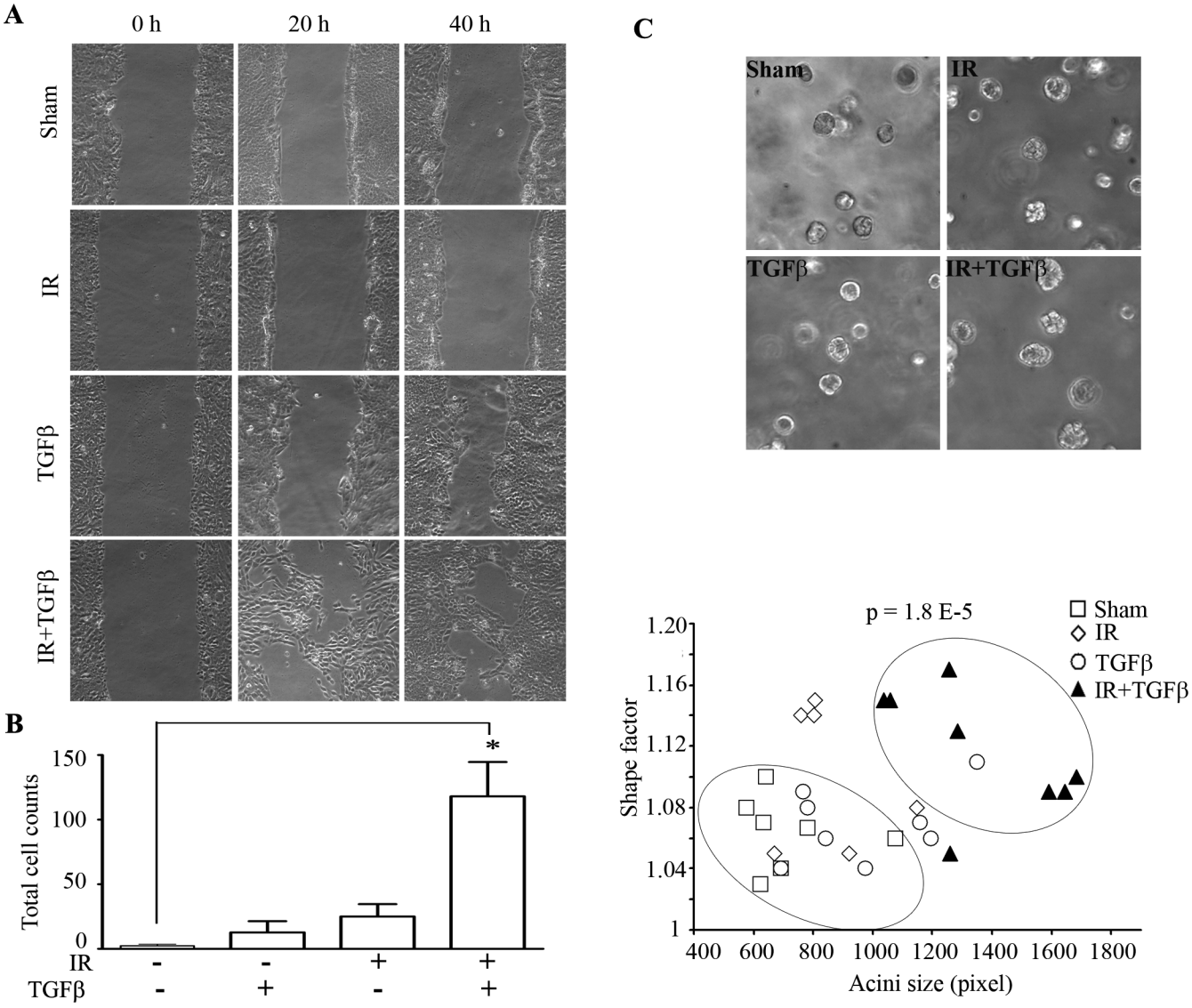
A
0 h
20 h
40 h
Sham
IR
TGFβ
IR+TGFβ
B
Total cell counts
150
100
50
0
*
IR
TGFβ
C
Sham
IR
TGFβ
IR+TGFβ
p = 1.8 E-5
Shape factor
1.20
1.16
1.12
1.08
1.04
1
400
600
800
1000
1200
1400
1600
1800
Acini size (pixel)

Figure 4

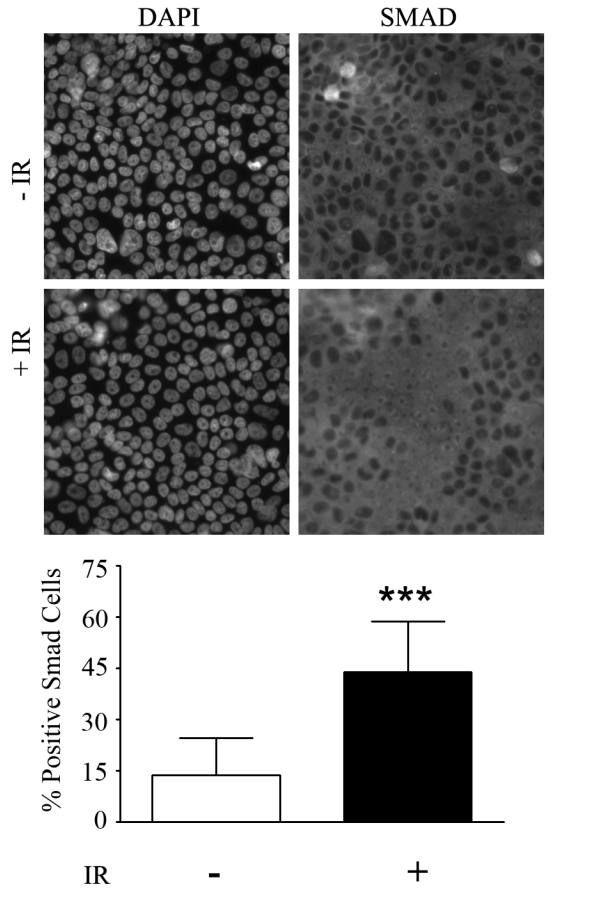
A
DAPI
SMAD
- IR
+ IR
% Positive Smad Cells
75
60
45
30
15
0
***
IR
-
+

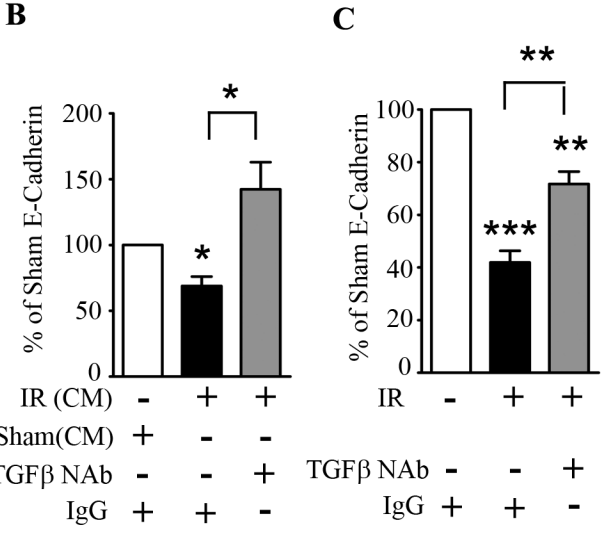
B
% of Sham E-Cadherin
200
150
100
50
0
*
*
IR (CM) - + +
Sham(CM) + - -
TGFβ NAb - - +
IgG + + -
C
% of Sham E-Cadherin
100
80
60
40
20
0
**
***
**
IR - + +
TGFβ NAb - - +
IgG + + -

Figure 5

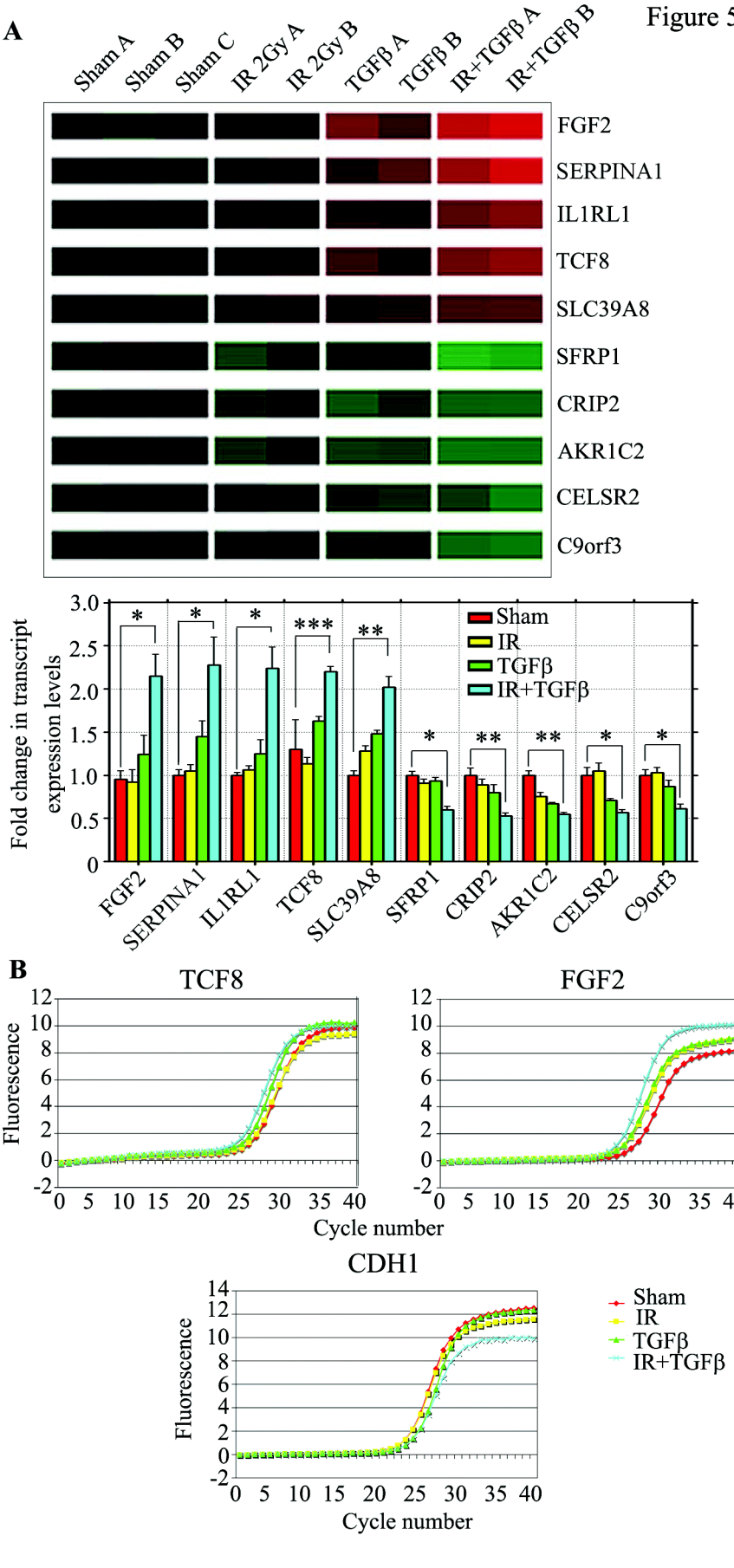
A
Sham A
Sham B
Sham C
IR 2Gy A
IR 2Gy B
TGFβ A
TGFβ B
IR+TGFβ A
IR+TGFβ B
FGF2
SERPINA1
IL1RL1
TCF8
SLC39A8
SFRP1
CRIP2
AKR1C2
CELSR2
C9orf3
Fold change in transcript expression levels
Sham
IR
TGFβ
IR+TGFβ
B
TCF8
FGF2
Fluorescence
Cycle number
CDH1
Sham
IR
TGFβ
IR+TGFβ

Figure 6

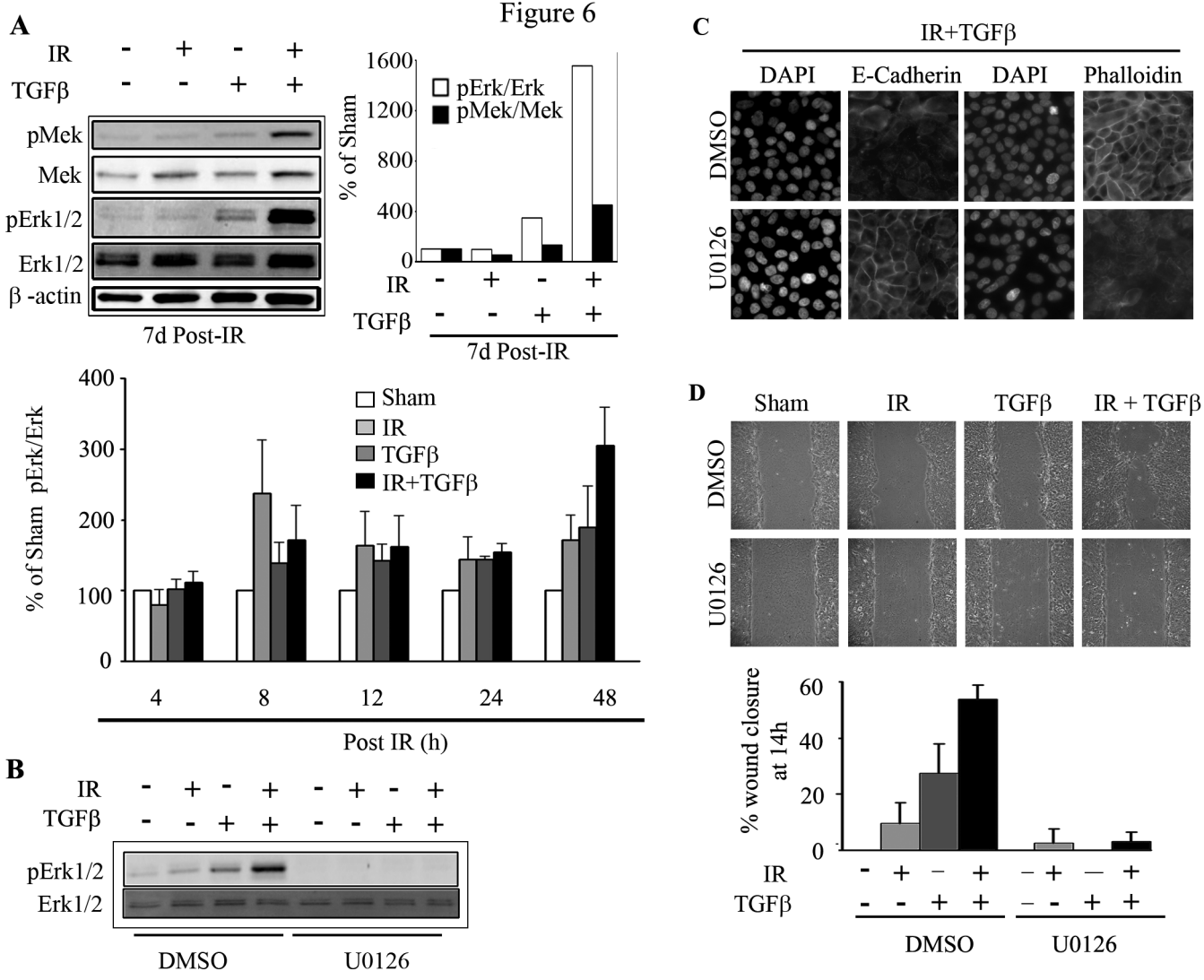
A
IR
TGFβ
pMek
Mek
pErk1/2
Erk1/2
β -actin
7d Post-IR
pErk/Erk
pMek/Mek
% of Sham
1600
1200
800
400
0
7d Post-IR
% of Sham pErk/Erk
Sham
IR
TGFβ
IR+TGFβ
400
300
200
100
0
4
8
12
24
48
Post IR (h)
B
pErk1/2
Erk1/2
DMSO
U0126
C
IR+TGFβ
DAPI
E-Cadherin
DAPI
Phalloidin
DMSO
U0126
D
Sham
IR
TGFβ
IR + TGFβ
DMSO
U0126
% wound closure at 14h
60
40
20
0
DMSO
U0126